Processing and Application of Ceramics 9 [4] (2015) 193–197
DOI: 10.2298/PAC1504193D

Characterization of cadmium substituted nickel ferrites prepared using auto-combustion technique

Manojit De, Aniruddha Mukherjee, Hari S. Tewari*

Department of Pure and Applied Physics, Advance Material Research Laboratory, Guru Ghasidas Vishwavidyalaya – Central University, Bilaspur, 495009, India

Received 9 September 2015; Received in revised form 19 December 2015; Accepted 23 December 2015

Abstract

In the present paper we have investigated synthesis of nickel ferrite ($NiFe_2O_4$) and cadmium substituted nickel ferrite ($Ni_{1-x}Cd_xFe_2O_4$) powders with particles' size in nanometer range using auto combustion technique as well as their sinterability. XRD analysis of the sintered samples confirmed the formation of single phase materials and the lattice parameter was increased with increase in cadmium concentration. It has also been observed that the estimated bulk densities of the materials decrease with increase in cadmium concentration, while they increase with the rise of sintering temperature.

Keywords: *nickel-cadmium ferrite, auto-combustion synthesis, sintering, XRD, FTIR*

I. Introduction

Nanocrystalline ferrites with general formula MFe_2O_4 (M = Ni, Co, Cu, Zn, Fe, Mn etc.) have several applications in technological fields: super ferro-fluids, magnetic resonance imaging enhancement, magnetic drug delivery, bio-molecule separation, colour imaging, magnetic high density storage, sensors and pigments [1–4].

Nickel ferrites are in demand for magnetic recording devices, magneto optical recording and electronic devices. Nickel ferrite ($NiFe_2O_4$) has spinel structure based on a face centred cubic lattice of the oxygen ions with the unit cell consisting of eight formula units. Metallic cations occupy the tetrahedral sites (A) and the octahedral sites (B) in the unit cell. Nickel ferrite ($NiFe_2O_4$) belongs to the class of ferrites with inverse spinel structure having structural formula $(Fe^{3+})[Ni^{2+}Fe^{3+}]O_4$. In inverse spinel structure, the Ni^{2+} ions together with half of the Fe^{3+} ions occupy B-sites and remaining half of the Fe^{3+} ions reside in tetrahedral A-sites. Magnetic interaction and distribution of cations among tetrahedral (A) and octahedral (B) sites have significant effects on the structural as well as electrical and magnetic properties [5,6].

In recent years, various methods have been developed to synthesize nanocrystalline ferrites including citrate precursor technology [7], micro-emulsion technology [8], co-precipitation [9], sol-gel [10], hydrothermal processes [11], etc. Synthesis of ferrites by conventional solid state reaction method involves higher calcination and sintering temperature which leads to the formation of inhomogeneity, poor stoichiometry and large crystallite size [12]. Amongst all methods used for synthesis of nanocrystalline materials, combustion method is one of the most popular, cheap and efficient low temperature technique that allows control over the chemical composition as well as densification of materials synthesized. Based on the property of matched oxidation and reduction between the fuel and oxidizer, the extremely safe combustion synthesis can be controlled through initial parameters. Depending upon the fuel and oxidizer, the temperature rises rapidly and as a result of auto-combustion, highly pure and crystalline nanosize materials are formed. Reaction between the mixture of nitrates and glycine results in a self-sustained exothermic process. This technique has associated advantages of getting soft and fine crystalline materials with high surface area and high purity at very low temperature (< 400 °C). The combustion method can be regarded as a thermally induced anionic redox reaction in the gel where the glycine behaves as reductant and nitrate ions as oxidant. Actually the glycine is acting as a fuel to propagate a self-propagating combustion syn-

*Corresponding author: tel: +91 094241 40587,
fax: +91 7752260154, e-mail: *tewari.hs@gmail.com*

thesis at low temperature. The basic principle of auto-combustion process is to distribute metal ions throughout the polymeric network and inhibit their segregation and precipitation.

In the present work we have investigated an interesting new process by adding metal nitrate - glycine in the molar ratio which resulted in lower ignition temperature for the formation of nanocrystalline phases. The nanostructures provide a high surface area and large amount of surface active sites for the reaction. Therefore, synthesis of nanostructures offers great potential to enhance the physical properties and widen the potential applications.

In order to tailor/control the physical properties of a material, tuning techniques including temperature, pressure and chemical substitutions are broadly employed. In MFe_2O_4 system, the magnetic and electrical properties can be varied by partial or full substitution of M^{2+} ions without losing crystalline nature. The cadmium substituted nickel ferrites are the magnetic materials characterized by maximum permeability, minimum hysteresis losses, temperature variation of properties between prescribed limits and low core losses at high frequencies, depending on their microstructure (density, porosity, size, shape) as well as macrostructure (crystal structure and elemental composition). However, not much work has been reported so far on Ni-Cd ferrites nanoparticles. Thus, in present work, we have reported synthesis of Ni-Cd ferrite nanoparticles using auto-combustion method, and investigated sinterability of the obtained powders.

II. Materials and methods

2.1. Synthesis

The calculation of molar ratio (fuel to oxidant ratio) has a significant role in redox based combustion synthesis. In the present work, the nitrates of the constituent materials were taken as oxidizer and glycine (NH_2CH_2COOH, Fine Chem Ltd. India, 99%) as fuel having molar ratio as 1 : 1.11.

In the present experimental procedure for the synthesis of $Ni_{1-x}Cd_xFe_2O_4$ [$0.0 \le x \le 0.6$] ferrites, first of all, stoichiometric amount of nickel nitrate (SD Fine Chem Ltd. India, 99%), cadmium nitrate (SD Fine Chem Ltd. India, 99%) and ferric nitrate (MERCK, India, 98%) salts were taken in a beaker and heated at 70 °C for 15–20 minutes until it gets completely melted. Then the glycine was added to this mixed solution and heated till it melts so as to get a homogeneous solution. The fully homogenized solution was further heated at higher temperature (320–350 °C, depending upon x) for 15 minutes resulting in combustion. At the end the obtained burned powder sample was crushed into powder form using mortar pestle. The synthesized Ni-Cd ferrites with various compositions were calcined at 800 °C for 6 hours in air. After cooling down to room temperature, the powders of various compositions were again ground and pelleted as a cylindrical pellets using hydraulic press at pressure of 5.5×10^4 N/m^2. These pellets were sintered at different temperatures at 1050 °C, 1100 °C and 1150 °C for 6 hours in air. Figure 1 shows the detail flowchart of experimental procedure.

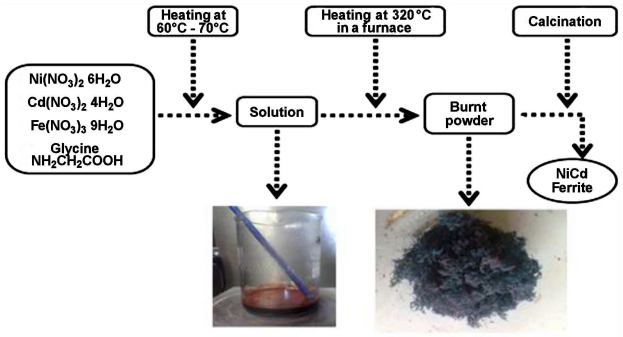

Figure 1. Flowchart of experimental procedure

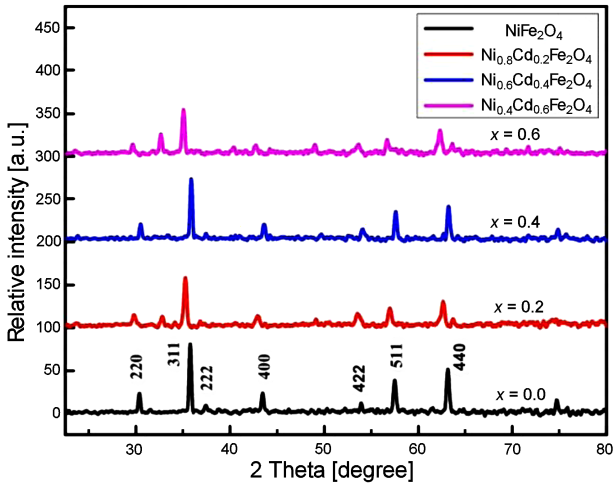

Figure 2. XRD patterns of $Ni_{1-x}Cd_xFe_2O_4$ ferrites sintered at 1050 °C as a function of cadmium concentration (x)

2.2. Characterization techniques

Structural analysis and phase identification of these ferrites were carried out by using X-ray diffraction technique on Rigaku, Miniflex diffractometer (Cu Kα radiation, $\lambda = 0.154056$ nm, $2\theta = 20$–$80°$). The average crystallite size (D in nm) was calculated from the XRD peak broadening of 311 peak by using Debye Scherrer's relation [13,14]:

$$D_{hkl} = \frac{k \cdot \lambda}{\beta \cdot \cos\theta} \tag{1}$$

where, $k = 0.9$ is the Scherrer's constant, $\lambda = 1.540562$ Å is wavelength of X-rays and β (in radian) is the full width of half maxima (FWHM) of the diffraction peak at an angle θ. The theoretical density (X-ray density) was calculated using the following relation:

$$\rho_{th} = \frac{Z \cdot M}{N \cdot a^3} = \frac{8M}{N \cdot a^3} \tag{2}$$

Here, $Z = 8$ represents the number of molecules per unit cell in the spinel lattice, M is the molecular weight of the ferrite, N and a are the Avogadro's number and lattice parameter, respectively [15].

The structural characterization was also performed with FTIR analysis. The spectra were recorded on the calcined samples by Shimadzu FT-IR 8400S equipment using KBr as reference material in a wave number region of 350 to 4000 cm^{-1}. The ratio of samples to KBr was taken as 95 : 5 and measured at room temperature.

Bulk density was calculated from geometrical volume and mass of the pellets. Porosity was calculated as the ratio of bulk and X-ray densities and densification parameter was determined by using the following equation $(\rho_{bulk} - \rho_0)/(\rho_{th} - \rho_0)$ were ρ_{bulk} is bulk density, ρ_{th} theoretical density and ρ_0 is density before sintering.

III. Results and discussion

3.1. XRD analysis

XRD patterns of the powdered $Ni_{1-x}Cd_xFe_2O_4$ (x = 0.0, 0.2, 0.4, 0.6) ceramics, obtained at room temperature, are shown in Fig. 2. The analysis of XRD patterns shows the formation of single phase compound of cubic spinel structure, since no other reflections are present, for all compositions sintered at 1050 °C. The lattice parameters, a_{exp}, for all samples were determined for the most prominent 311 peak of the XRD pattern and tabulated in Table 1. It is observed that the 311 peak position is displaced continuously towards lower angle. It is indicating a linear increase in the lattice parameter upon increasing cadmium content in nickel ferrite which is in good agreement with Vegard's law [16]. The larger ionic radii of Cd^{2+} (0.97 Å) to that of Ni^{2+} (0.69 Å) and Fe^{3+} (0.645 Å) results in an increase of the lattice parameter and expansion of the lattice cell.

The variations of average crystalline size and theoretical density (calculated from XRD data) with composition of the prepared Ni-Cd ferrites are shown in Table 1. Theoretical density, calculated using the lattice parameter of the samples sintered at 1050 °C, increases with cadmium concentration (Table 1) due to the larger atomic weight of cadmium. However, there is no considerable change of average crystallite size with cadmium addition.

3.2. Density, porosity and densification parameters

The variations of bulk density (ρ_{bulk}) with cadmium concentration, for the pellets sintered at 1050 °C, 1100 °C and 1150 °C, are given in Table 1. The bulk density decreases with increase in cadmium concentration, but increases with increase in sintering temperature. Accordingly, the apparent porosity of the investigated samples decreases with increase in sintering temperature (Table 1) and increases with cadmium concentration, similarly as reported in literature [17]. It is important to mention that high portion of porosity remained in the ferrite samples even after sintering at 1150 °C.

3.3. FTIR analysis

FTIR analysis was used to identify unknown materials as well as to determine the quality or consistency of a sample and the amount of components. Figure 3 shows the recorded spectra of cadmium substituted nickel ferrite samples in 450 to 3700 cm^{-1} range.

Depending on the mass of metal cations and strength of the bond between metal cations and oxygen absorption occurred at different frequencies. As reported in literature [18], the FT-IR bands of solids in the range of 1000–100 cm^{-1} are usually assigned to vibration of ions in the crystal lattice. Since Ni^{2+} ions occupied octahedral B sites in nickel ferrites, the substitution with Cd^{2+} ions decreases the amount of Ni^{2+} ions and redistributes Fe^{3+} ions from B site to A site. This causes shifting of the band positions toward lower wave numbers.

In all spinel ferrites, two main broad metal oxygen bands are seen in the FTIR spectra [19–22]. Therefore the highest one, observed around ν_1 = 606 cm^{-1} (inset in Fig. 3), corresponds to intrinsic stretching vibra-

Table 1. Variation of lattice parameter (a_{exp}), crystallite size (D_{hkl}), X-ray density (ρ_{th}), bulk density (ρ_{bulk}), densification parameter (α) and porosity of $Ni_{1-x}Cd_xFe_2O_4$ ceramics

Cadmium concentration, x	Sintering temperature [°C]	Lattice parameter [Å]	Crystallite size [nm]	X-ray density [g/cm^3]	Bulk density [g/cm^3]	Densification parameter	Porosity [%]
0.0	1050	8.338	29.2	5.370	2.766	0.000	48.49
	1100				2.872	0.041	46.51
	1150				3.050	0.109	43.20
0.2	1050	8.343	27.8	5.606	2.705	0.000	51.47
	1100				2.722	0.006	51.45
	1150				2.778	0.025	50.45
0.4	1050	8.361	29.9	5.813	2.674	0.000	53.99
	1100				2.681	0.002	53.88
	1150				2.690	0.005	53.72
0.6	1050	8.379	32.9	5.985	2.637	0.000	55.94
	1100				2.648	0.003	55.76
	1150				2.684	0.014	55.16

Table 2. Absorption band frequency and force constant of $Ni_{1-x}Cd_xFe_2O_4$

Cadmium concentration, x	ν_t [cm^{-1}]	ν_o [cm^{-1}]	K_t [10^2 N/m]	K_o [10^2 N/m]
0.0	606	460	2.72	1.55
0.2	593	462	2.60	1.57
0.4	594	464	2.61	1.58
0.6	595	465	2.62	1.59

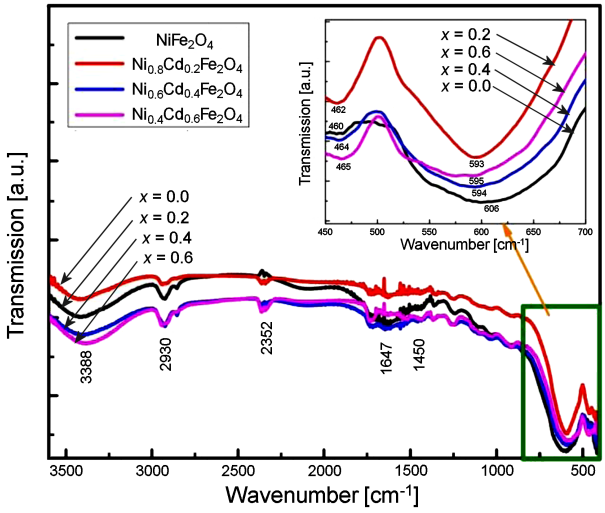

Figure 3. FT-IR spectra of $Ni_{1-x}Cd_xFe_2O_4$ at four different cadmium concentrations (x) at room temperature

tions of the metal ion at the tetrahedral site, (M_{tetra}–O; $Cd^{2+}\leftrightarrow$O), whereas the lowest band, that observed around ν_2 = 460 cm^{-1} is assigned to octahedral metal stretching vibration (M_{octa}–O; $Fe^{3+}\leftrightarrow$O and $Ni^{2+}\leftrightarrow$O) [20]. Inset in Fig. 3 shows a difference in the peak positions of ν_1 and ν_2 absorptions bands that may be due to change of bond length with increase of cadmium concentration. The band appearing at 3388 cm^{-1} corresponds to O–H stretching vibration of H_2O; the special absorption peak at 2930 cm^{-1} corresponds to O–H group of citric acid; the band at 1450 cm^{-1} corresponds to antisymmetric NO_3 stretching vibrations and the band at 1647 cm^{-1} corresponds to carbo-oxalate anions [19–22]. The stretching vibration at 2352 cm^{-1} corresponds to the hydroxyl group.

The force constant is the second order derivative of potential energy with respect to site radius. The estimation of the force constant of the tetrahedral (K_t) and octahedral site (K_o) have been performed for these two vibrational bands (ν_1 and ν_2) by employing the method suggested by Waldron [20] as given by following equation:

$$K = 4\pi^2 \cdot C^2 \cdot M \cdot \nu^2 \qquad (3)$$

where, M represents the atomic mass of the cations occupying tetrahedral and octahedral sites, ν is the corresponding wave number and C is speed of light in free space. Table 2 contains the calculated values of K_t and K_o. The tetrahedral force constant at first decreases then gradually increases with cadmium concentration whereas octahedral force constant increases in this ferrite system as reported for similar systems [23–25]. Thus, substitution of Ni^{2+} with Cd^{2+} ions in tetrahedral site redistributes Fe^{3+} ion from tetrahedral to octahedral site and results in a charge imbalance on the system increase tetrahedral force constant.

IV. Conclusions

The present work includes the synthesis of Ni-Cd ferrites at different cadmium concentration using autocombustion method and sintering of the obtained samples. It has been observed that due to shrinkage during sintering, the estimated bulk density of the materials increases from 2.63 to 2.73 g/cm^3. XRD analysis of the sintered Ni-Cd ferrites confirmed the formation of single phase materials and estimated the lattice parameters between 8.34–8.37 Å, XRD density from 5.37 to 5.98 g/cm^3 and crystallite size from 27 to 33 nm. The observed results for host Ni-ferrite are in good agreement with the reported data.

Acknowledgemets: Authors are thankful to Department of Pure and Applied Physics, Guru Ghasidas Vishwavidyalaya for facilities. One of us (HST) is thankful to University Grant Commission, New Delhi, India, for financial assistance through MRP (F. No. 41-954/2012(SR)). MD is thankful to UGC for his fellowship.

References

1. S.K. Shrivastava, N.S. Gajbhiye, "Low temperature synthesis, structural, optical and magnetic properties of bismuth ferrite nanoparticles", *J. Am. Ceram. Soc.*, **95** (2012) 3678–3682.
2. M.A. Gabal "Non-isothermal decomposition of NiC_2O_4–FeC_2O_4 mixture aiming at the production of $NiFe_2O_4$", *J. Phys. Chem.*, **64** (2003) 1375–1385.
3. M.P. Pileni, "Magnetic fluids: Fabrication, magnetic properties, and organization of nanocrystals", *Adv. Funct. Mater.*, **11** [5] (2001) 323–336.
4. E.C. Smelling, *Soft Ferrites: Properties and Applications*, Iliffe Book Ltd., London, 1969.
5. L.L. Hench, J.K. West, *Principles of Electronic Ceramics*, Wiley, New York, 1990.
6. P. Cousin, R.A. Ross, "Preparation of mixed oxide: A review", *Mater. Sci. Eng. A*, **130** (1990) 119–125.
7. M. Mouallem-Bahout, S. Bertrand, O. Peña, "Synthesis and characterization of $Zn_{1-x}Ni_xFe_2O_4$ spinels prepared by a citrate precursor", *J. Solid State*

Chem., **178** (2005) 1080–1086.
8. R.D.K. Misra, A. Kale, R.S. Srivastava, O.N. Senkov, "Synthesis of nanocrystalline nickel and zinc ferrites by microemulsion technique", *Mater. Sci. Technol.*, **19** (2003) 826–830.
9. G. Vaidyanathan, S. Sendhilnathan, "Characterization of $Co_{1-x}Zn_xFe_2O_4$ nanoparticles synthesized by co-precipitation method", *Physica B: Condens. Matter*, **403** (2008) 2157–2167.
10. A.T. Raghavender, N. Biliškov, Ž. Skoko, "XRD and IR analysis of nanocrystalline Ni-Zn ferrite synthesized by the sol-gel method", *Mater. Lett.*, **65** (2011) 677–680.
11. Z. Wang, Y. Xie, P. Wang, Y. Ma, S. Jin, X. Liu, "Microwave anneal effect on magnetic properties of $Ni_{0.6}Zn_{0.4}Fe_2O_4$ nano-particles prepared by conventional hydrothermal method", *J. Magn. Magn. Mater.*, **323** (2011) 3121–3125.
12. A.E. Smith, H. Mizoguchi, K. Delaney, N.A. Spaldin, A.W. Sleight, M.A. Subramanian, "Mn^{3+} in trigonal bipyramidal coordination: A new blue chromophor", *J. Am. Chem. Soc.*, **131** (2009) 17084–17086.
13. H.P. Klung, L.B. Alexander, *X-ray Diffraction Procedures*, Wiley, New York, 1974 (p. 687).
14. B.D. Cullity, *Elements of X-ray Diffraction*, Addison-Wesley Publishing Company, Inc., Philippines, 1978, (p. 284).
15. I.H. Gul, A.Z. Abbasi, F. Amin, M. Anis-ur-Rehman, A. Maqsood, "Structural, magnetic and electrical properties of $Co_{1-x}Zn_xFe_2O_4$ synthesized by co-precipitation method", *J. Magn. Magn. Mater.*, **311** (2007) 494–499.
16. C.G. Winfrey, D.W. Eckart, A. Tauber, "Preparation and X-ray diffraction data for some rare earth stannets", *J. Am. Chem. Soc.*, **82** (1960) 2695–2697.
17. M.B. Shelar, P.A. Jadhav, S.S. Chougule, M.M. Mallapur, B.K. Chougule, "Structural and electrical properties of nickel cadmium ferrites prepared through self-propagating auto combustion method", *J. Alloys Compd.*, **476** (2009) 760–764.
18. M. Salavati-Niasari, F. Davar, T. Mahmoudi, "A simple route to synthesize nano-crystalline nickel ferrite ($NiFe_2O_4$) in the presence of octanoic acid as a surfactant", *Polyhedron*, **28** [8] (2009) 1455–1458.
19. T. Shanmugavel, S. Gokul Raj, G. Ramesh Kumar, G. Rajarajan, D. Saravanan, "Cost effective preparation and characterization of nano-crystalline nickel ferrites ($NiFe_2O_4$) in low temperature regime", *J. King Saud University - Science*, **27** (2015) 176–181.
20. R.D. Waldron, "Infrared spectra of ferrites", *Phys. Rev.*, **99** [6] (1955) 1727–1735.
21. N.W. Grimes, A.J. Collett, "Infrared absorption spectra of ferrites", *Nature Phys. Sci.*, **230** (1971) 158.
22. K. Nejati, R. Zabihi, "Preparation and magnetic properties of nano size nickel ferrite particles using hydrothermal method", *Chem. Central J.*, **6** (2012) 23 (6 pages).
23. H.A. Dawoud, S.K. Shaat, "A structural study of Cu-Zn ferrites by infrared spectra", *Al-Aqsa Unversity Journal*, **10** (2006) 247–262.
24. K.B. Modi, J.D. Gajera, M.P. Pandya, H.G. Vora, H.H. Joshi, "Far-infrared spectral studies of magnesium and aluminum co-substituted lithium ferrite", *Pramana- J. Phys.*, **62** [5] (2004) 1173–1180.
25. M.C. Chhantbar, U.N. Trivedi, P.V. Tanna, H.J. Shah, R.P. Vara, H.H. Joshi, K.B. Modi, "Infrared spectral studies of Zn-substituted $CuFeCrO_4$ spinel ferrite system", *Indian J. Phys.*, **78A** [3] (2004) 321–326.